doi:10.1016/j.jmb.2004.10.084 J. Mol. Biol. (2005) 345, 837–854

JMB

Available online at www.sciencedirect.com

SCIENCE DIRECT®

ELSEVIER

The Requirement for Mechanical Coupling Between Head and S2 Domains in Smooth Muscle Myosin ATPase Regulation and its Implications for Dimeric Motor Function

Florence Tama[1], Michael Feig[1], Jun Liu[2], Charles L. Brooks III[1] and Kenneth A. Taylor[2]*

[1]*Department of Molecular Biology, TPC6, The Scripps Research Institute, 10550 North Torrey Pines Road, La Jolla CA 92037, USA*

[2]*The Institute of Molecular Biophysics, Florida State University, Tallahassee, FL 32306-4380, USA*

**Corresponding author*

A combination of experimental structural data, homology modelling and elastic network normal mode analysis is used to explore how coupled motions between the two myosin heads and the dimerization domain (S2) in smooth muscle myosin II determine the domain movements required to achieve the inhibited state of this ATP-dependent molecular motor. These physical models rationalize the empirical requirement for at least two heptads of non-coiled α-helix at the junction between the myosin heads and S2, and the dependence of regulation on S2 length. The results correlate well with biochemical data regarding altered conformational-dependent solubility and stability. Structural models of the conformational transition between putative active states and the inhibited state show that torsional flexibility of the S2 α-helices is a key mechanical requirement for myosin II regulation. These torsional motions of the myosin heads about their coiled coil α-helices affect the S2 domain structure, which reciprocally affects the motions of the myosin heads. This inter-relationship may explain a large body of data on function of molecular motors that form dimers through a coiled-coil domain.

Keywords: coiled coil; phosphorylation; light chains; homology model; elastic network

Introduction

Myosin II is the predominant molecular motor in smooth muscle cells. Like all myosin II isoforms, it has a pair of heavy chains (HC), two pairs of light chains (LC), the essential or ELC and the regulatory or RLC and can form filaments.[1] The N-terminal ~850 residues of the HC form a globular head, the S1 domain, the first segment of which, called the motor domain, contains the ATPase and actin-binding activities. This is followed by a long α-helix, to which the light chains bind, thereby forming a lever arm that amplifies movements in the motor domain to produce the power stroke in muscle.[2] The remainder of the HC forms a long, predominantly coiled coil, α-helical domain known as the myosin rod. The first approximately one-third of the myosin rod, the S2 domain, contains the HC dimerization activity and the rest, the LMM, the filament-forming activity.

The actin activated ATPase of smooth muscle myosin II is regulated by phosphorylation of S19 of the RLC;[3] ATPase activity is low in the dephosphorylated (inhibited) state. RLC phosphorylation increases the ATPase activity up to 1000 fold,[4] but the structural mechanism of activation is unknown. Extensive studies of smooth muscle myosin regulation have elucidated several key features. Only intact myosin and the soluble two-headed fragment, smHMM, show high levels of regulation[5] implying that the inhibited state requires an interaction between myosin heads. This interaction

Present address: M. Feig, Department of Biochemistry and Molecular Biology, Michigan State University, East Landing, MI 48824-1319, USA.

Abbreviations used: HC, heavy chain; LC, light chain; ELC, essential light chain; RLC, regulatory light chain; HMM, heavy meromyosin; smHMM, soluble two-headed fragment of smooth muscle myosin; LMM, light meromyosin; NMA, normal mode analysis.

E-mail address of the corresponding author: taylor@bio.fsu.edu

0022-2836/$ - see front matter

was observed recently by cryoelectron microscopy,[6] which revealed an asymmetrical head–head interaction (Figure 1(b)). In the inhibited structure, the motor domain of one S1, the "blocked" head, interacts with the motor domain, the converter domain (HC residues G720–G779), and the ELC of the other S1, the "free" head (Figure 1(b)). The free head can be docked onto actin without steric interference, but the blocked head cannot, thereby explaining the retention of actin binding in the inhibited state.[7]

Dimer formation alone is not sufficient for complete regulation. In addition, a minimal S2 length of ~140 residues and a minimum of two heptads of uncoiled α-helix at the S1–S2 junction are necessary.[8,9] Moreover, it is the length of S2 alone that is most important; the sequence itself seems to be less important.[8,10] How the S2 structure affects the interaction of the myosin heads is unknown.

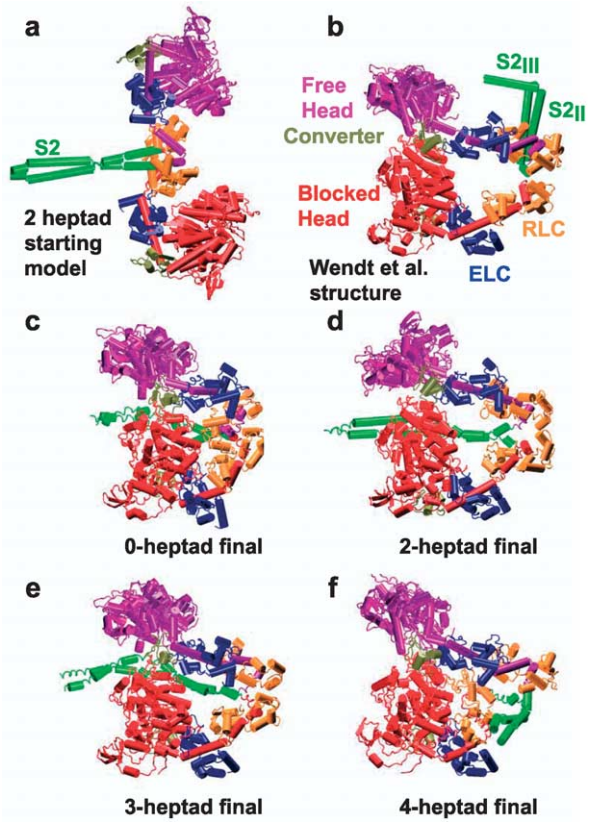

Figure 1. Models for smHMM. (a) Starting, two-heptad active-state model. The color scheme used throughout has the S2 domain in green, "free" S1 HC in magenta, "blocked" head HC in red, ELC in blue, RLC in gold and converter domain in brown. (b) The inhibited-state structure, which juxtaposes the actin-binding region of the blocked head, with the free head upper 50 kDa, converter and ELC. S2 segments $S2_{III}$ and $S2_{II}$ are labelled. The $S2_{III}$ density in the actual 3-D map has a left-handed twist to it. The $S2_{II}$ density is too short to show this. The $S2_{I}$ segment is not shown, since it was not resolved in the original reconstruction.[6] (c–f) Inhibited-state smHMM models obtained from NMA. (c) No uncoiled heptad before the S2 coiled coil; (d) two heptads; (e) three heptads; and (f) four heptads. In this model, the S2 extends up out of the plane of the page.

It is clear that the interaction between myosin heads is modified by the structure of S2, but it is likely that the stable interaction between the myosin heads affects reciprocally the structure of S2 and, through it, the myosin rod. *In vitro* at physiological ionic strength, ATP binding to dephosphorylated smooth muscle myosin filaments causes them to dissolve. The dissolved myosin adopts a bent-hairpin conformation,[11] referred to as the 10 S form, that is unsuitable for filament formation. The detailed arrangement of the myosin heads in the 10 S form is the same as that in the inhibited state of smHMM,[12] implying that the head–head interaction affects the rod structure, destabilizing the filaments and promoting the 10 S form. Phosphorylation of the RLC causes a conformational change in the S1 heads that disrupts the head–head interaction, leading to an extended structure for the myosin rod that is competent for filament assembly.[11,13,14] ATP binding and RLC phosphorylation affect ATPase activity and solubility of myosin II from non-muscle cells in a similar way.[15] Another class of "regulated" myosin, from the striated adductor muscle of scallop, exhibits similar behavior but in response to Ca^{2+} rather than RLC phosphorylation,[16,17] and shows a similar head–head interaction to dephosphorylated smHMM.[18]

These experimental results imply coupling between the head–head interaction and the coiled-coil domain such that the structure of one has important effects on the other. The present modelling study was undertaken to provide a theoretical framework within which this coupling could be understood and thereby used to explain observations and predict features in myosin and other two-headed motors that involve a coiled-coil domain. The effort is unique, in that we use the motions of the two S1 heads to predict movements and structural changes in the coiled-coil domain that correlate well with the biochemistry of smooth muscle myosin regulation.

Results

All of the structural models used for the initial state are similar to that shown in Figure 1(a) and differ mainly in the separation between the two S1 domains, which increases with the number of non-coiled heptads. Since the two motor domains are separated widely, the initial state would correspond to an "active-state" conformation.[11,13] However, we envision this active-state model corresponding to the beginning of the conformational change to the inhibited state, i.e. following dephosphorylation of the RLC. The inhibited-state conformation was based on a crystallographically refined version of the Wendt *et al*. structure (PDB 1I84) that had been modified to contain an homology model for the HC-RLC domain based on the smooth muscle sequence (Figure 1(b)).[12] We used only the S1

coordinates from this refined structure in our modelling to permit us to explore the final position of S2 following a transition from the active and inhibited conformations. Thus, all the movements of S2 observed in our models result from coupled motions with the myosin heads.

In this study, we use normal mode analysis (NMA) to investigate the transition between active-state and inhibited-state conformations. NMA is a powerful technique with which to study dynamics of large biomolecules.[19] The normal modes provide information on the natural vibrations of the molecule and the preferential directions of collective, many atom displacements. The extent and direction of functionally important large-scale molecular rearrangements observed experimentally are often well represented by a small number of the lowest-frequency, highest-amplitude normal modes.[20,21] On this basis, we argue that correct putative active-state models can be distinguished from less correct models by the ability to conform those models to the final inhibited state along a small number of low-frequency normal modes. Moreover, the amount of strain introduced into the molecule from the transition provides information on the ease with which the conformational change is anticipated to occur.

Structural requirements

After the conformational change, the arrangement of the myosin motor domains for all the final models is very similar to the inhibited-state structure (Figure 1(c)–(f)); it is the arrangement of the RLCs that differs the most. The RLC positions in the two-heptad and three-heptad models are closest in appearance to the inhibited state structure and the zero-heptad and four-heptad models are clearly very different. The zero-heptad active-state model differs from the other active-state models in that the RLC domains are in van der Waals contact and the beginning of the coiled coil is at the S1–S2 junction. All the other initial models have separation between the two RLCs, allowing independent movement of the two S1 domains. The inhibited-state structure juxtaposes the N-terminal domains of the two RLCs, but these are juxtaposed to the C-terminal domains in the starting zero-heptad model. The S1 heads in the zero-heptad model must slide in opposite directions to achieve the correct RLC alignment (Figure 1(b)), but initiation of the coiled coil so close to the S1–S2 junction results in a structure ill-suited to this movement.

In addition to incorrect relative placement of the RLCs, the final four-heptad model (Figure 1(f)) also had its S2 domain oriented perpendicular to the S1 heads; a placement inconsistent with electron microscopy observations.[11,13] Together, these findings suggest that two or three heptads of non-coiled α-helix at the S1–S2 junction are optimal to achieve the coupling of the S1 and S2 domains needed to produce the conformational change from an active form to an inhibited form. This result agrees with a recent crystal structure of the first 51 residues of S2 from scallop myosin,[22] which showed that the first two heptads of S2 formed an unstable coiled coil.

Quantitatively, convergence to the inhibited-state structure of smHMM was optimal for two-heptad or three-heptad active-state models (Table 1). The deviations of the two-heptad and three-heptad models are within acceptable limits for docking to the 20 Å resolution cryo electron microscopy data,[23] which is the resolution at which the inhibited-state structure was produced. The conformational change deposits strain energy into both S1 and S2 domains. The strain energy for the overall model paralleled the rms deviation (Table 1); it was less for the two-heptad model than the three-heptad model but lowest for the four-heptad model, which was not conformed correctly to the inhibited conformation. In addition, considering only the S1 domains of the two-heptad final model as a single rigid body, fits to 3-D reconstructions of inhibited smooth muscle myosin and smHMM[6,12] yielded correlation coefficients of 0.74 and 0.72, comparable to the value obtained for the refined inhibited structure.

The S2 placement in our two-heptad inhibited-state model differs from that reported by Wendt *et al.*, which had the obvious S2 segment, $S2_{III}$ (Figure 1(b)), located to the outside of the free head.[6] To examine this aspect further, we overlaid and scaled our two-heptad inhibited-state model onto the electron density map provided by Wendt *et al*. The S2 placement aligns in projection near the $S2_{III}$ domain, but one or two unit cells away from that containing the two S1 heads (Figure 2(a)). In a second comparison, we aligned the same two-heptad inhibited state model with the 3-D reconstruction of 10 S smooth muscle myosin.[12] In this case, S2 was located close to well-resolved density between the two S1 heads but unconnected to the S1–S2 junction (Figure 2(b)). The S2 placement obtained from NMA, close to appropriate density in the 3-D images, is strong evidence for the validity of this model over that proposed by Wendt *et al.*, and is consistent with averaged images of dephosphorylated smHMM preserved in negative stain.[24]

Experimentally, it is known that the RLC N termini are necessary to stabilize the 10 S conformation of whole myosin,[25] but it is less clear that they are needed to stabilize the inhibited state of smHMM. The positioning of the S2 domain with respect to the S1 heads in the two-heptad and three-heptad inhibited-state models shows that the motion of the heads by itself is sufficient to place the S2. The modelling suggests that the N-terminal residues of the RLC are not needed to achieve this position and may not be necessary to stabilize it in smHMM. F25, which in the smooth muscle RLC corresponds to the first residue seen in the S1 crystal structures, on both the free and blocked head RLCs does not appear to be placed well for an interaction with S2. In both cases, the C^{α}–C^{α} "bond" between F25 and D26, and helix-1, to which it connects, point

Table 1. Structural parameters after the active to inhibited transformation

Model[a,b]	RMS deviation (Å)[c]	Δ Secondary structure[d]	Domain RMS deviation (Å)[e]	σ C^{α}–C^{α} (Å)[f]	Relative bond strain energy[g]
Zero-heptad$_{1105}$	13.6				1
S1		0.081	2.51	0.144	
S2 (852–931)		1.066		0.327	
S2 (852–1105)		0.723		0.312	
Two-heptad$_{1105}$	6.3				0.67
S1		0.120	2.05	0.133	
S2 (852–931)		0.848		0.266	
S2 (852–1105)		0.340		0.245	
Three-heptad$_{1105}$	8.2				0.75
S1		0.157	2.81	0.156	
S2 (852–931)		1.145		0.414	
S2 (852–1105)		0.476		0.285	
Four-heptad$_{1105}$	12.2				0.60
S1		0.140	4.01	0.191	
S2 (852–931)		0.842		0.287	
S2 (852–1105)		0.314		0.182	

[a] Subscripts indicate the number of heavy-chain residues used in the model.
[b] Numbers in parentheses indicate the range of residues within S2 used in the calculation, i.e. 852–931, 852–1105 etc.
[c] RMS deviation is relative to the inhibited structure, which was based on PDB 1I84.
[d] Secondary structure determined using MOLAUTO.[92] Change is calculated using $R = \Sigma|F_i - F_f|/\Sigma|F_i|$, where the summation is over four classes of secondary structure; coil, helix, sheet and turn. F_i and F_f are the fraction of the particular secondary structure in the initial and final models respectively.
[e] RMS deviation calculated over four S1 domains: HC residues 2–719, 720–790, ELC and its bound heavy chain (residues 791–815), and RLC and its bound heavy chain (residues 816–851). S2 is assumed to start at HC residue 852.
[f] Average C^{α}–C^{α} distances stayed very uniform, usually between 3.8 Å and 3.9 Å. The value for the initial model was 3.85($\pm$0.05) Å.
[g] Calculated from equation (1) using $C = 1.0$. The energies were normalized, i.e. the largest energy, that for the zero-heptad model, was set to 1.

away from S2. However, the RLC N termini may play a role in stabilizing the 2-D arrays. When the two-heptad inhibited-state model is overlaid on the inhibited-state smHMM density map (Figure 2(a)), F25 of the free head RLC is close to the density attributed by Wendt *et al*. to $S2_{II}$. This density connects to the $S2_{III}$ density, suggesting that it may instead be due to the RLC N terminus and may be stabilizing the 2-D arrays by interacting with an S2 domain from another molecule.

In the 10 S myosin 3-D map (Figure 2(b)), there is density due to myosin rod in this same location near the free head, although the density linking it to the RLC is not as well defined. If we interpret the rod density near the free head by analogy with the smHMM reconstructions described above, any connection would be intermolecular. Perhaps more interesting is a density near F25 of the blocked head RLC. This density is not seen in the smHMM reconstructions and may also be due to myosin rod. A potential interaction here might be intramolecular in nature. Without building in the S2 and rod sequence into both of the reconstructions, it is not possible to determine which regions of rod are potentially interacting with the free head RLC or whether the potential connection between rod and the blocked head RLC is an intra- or intermolecular interaction.

The structure of myosin at the S1–S2 junction is predicted to be entirely α-helical.[26] To test whether the coupled movement between S1 and S2 *requires* the protein structure to be α-helical, we modified the two-heptad active-state model by changing five residues of the helix after the S1–S2 junction to a β-strand conformation. NMA showed that movements of the S1 and S2 domains are decoupled in this model; S1 could not be conformed to the inhibited-state structure and the S2 domain could not be conformed to a location between the myosin heads. Our modelling, therefore, suggests that if the S2 domain is entirely α-helical and contains two or three heptads of non-coiled α-helix at the S1–S2 junction, then the head–head interaction is sufficient to form the inhibited conformation. A helix break at the S1–S2 junction is not required. Indeed, a continuous α-helix appears to be necessary to achieve the coupled displacements of S1 and S2 toward the inhibited conformation.

Strain in the conformational change

In the starting, active-state model, the lever arms of the two S1 heads are 180° apart but are ~30° apart after the conformational change. Much of the ~150° difference must be taken up by the S2 domain. To evaluate the distortions induced by this twisting motion, we calculated the bond strain in the final model using equation (1) and the elastic network defined by the initial model.[27] The conformational change produces strain in both S1 and S2. The strain for the overall model paralleled the rms deviation (Table 1); it was less for the two-heptad model than the three-heptad model but lowest for the four-heptad model, which was not conformed correctly to the inhibited conformation. When the distribution of strain in the myosin HC is calculated for the two-heptad final model, it is found to be greatest at the S1–S2 junction and along the initial

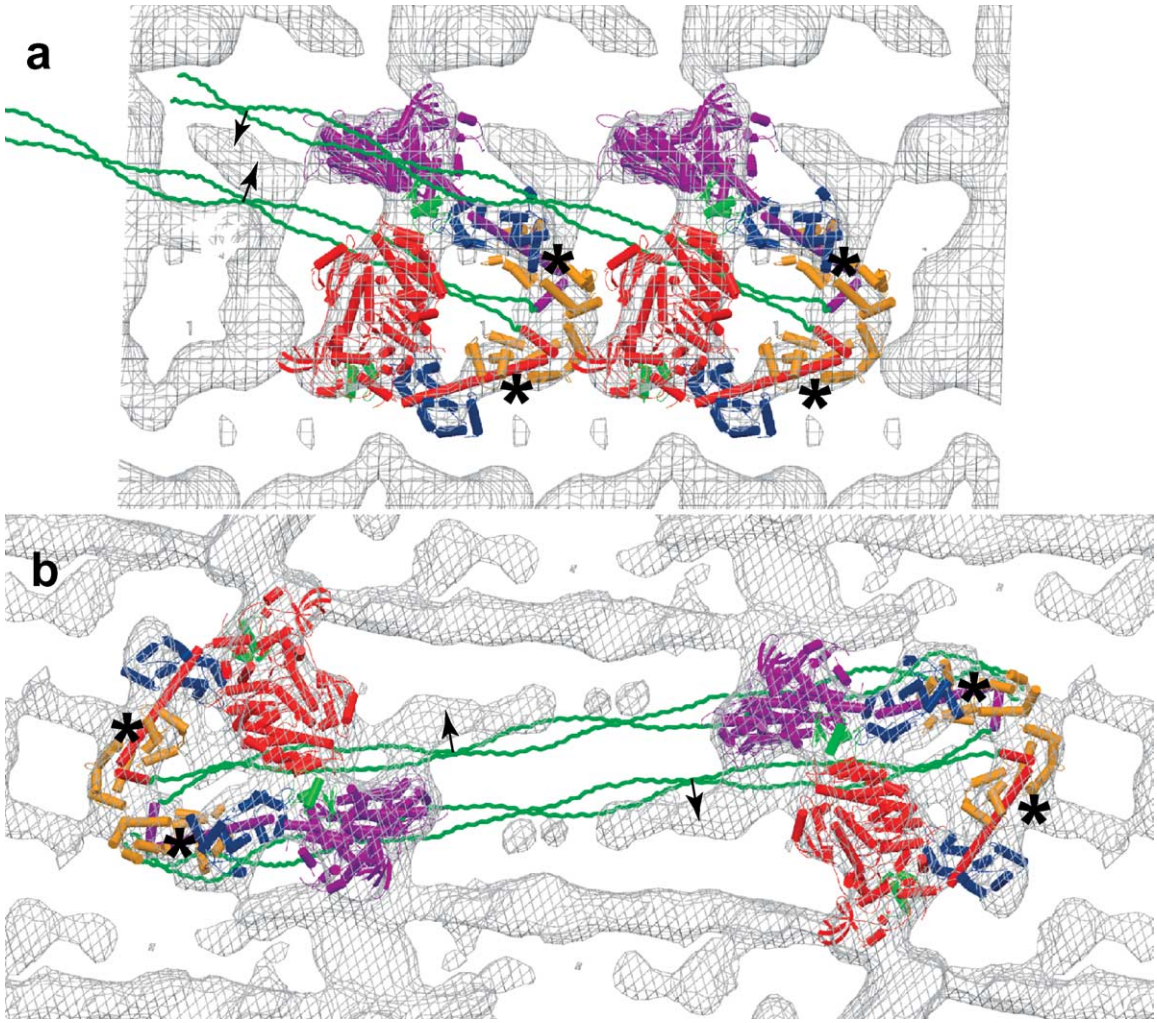

Figure 2. Placement of the S2 domain after NMA within cryoEM 3-D images of smHMM[6] and 10 S myosin.[12] (a) In smHMM, the S2 model aligns near the S2 density, but either one or two unit cells from the one containing the S1 domains. (b) The 10 S smooth muscle myosin array. The S2 model aligns with a density below the blocked head, unconnected with the S1–S2 junction. Other density, probably the LMM domain, remains unassigned. Asterisks (*) in (a) and (b) indicate the location of F25, the first residue in the RLC models. In (b) F25 of the blocked head lies almost on top of density that is probably due to myosin rod. The Figure is displayed using MOLSCRIPT.[92]

segment of S2 (Figure 3). A secondary point of strain is found on the HC between the RLC and the ELC.

To examine the motions that produce this strain, we aligned the two-heptad active-state model with the inhibited state structure using the first two heptads of the S2 domain. This is the only axis that can reasonably relate torsional motions of the two heads. Considering the differences between the initial and final states, these two segments of the HC align quite well (2.4 Å rms deviation for 28 atoms). The motion at the S1–S2 junction consists of both twisting and bending components. The twisting motion for both S1 heads toward the inhibited state model (Figure 4(a)) is in an anticlockwise direction with respect to the helix axis (note that the S2 axis is pointing down in the Figure). The blocked head twist is greater in magnitude than that of the free head (135° *versus* 110°). The conformational change increases an ~30° bend between the "hook" domain and the S2 domain to ~60° for both heads in the inhibited state model (Figure 4(b)).

Changes in the blocked head itself consist mainly of a decrease in the HC bend between the ELC and the RLC (40° to 20°). The corresponding change for the free head is greater and additionally involves a clockwise twist of the RLC-HC domain about the bend in the HC at the ELC (Figure 4(c)). For both heads, the direction of this bend is toward the target inhibited structure but goes beyond it by 10–20°. In the free head, the bend between the converter and the ELC is increased as was previously observed.[6] Thus, the changes in the free head are greater than for the blocked head but the torsional motion at the S1–S2 junction is greater for the blocked head than the free head.

As the starting smHMM models are conformed to the inhibited structure, the secondary structure is changed and some C^{α}–C^{α} distances are stretched while others are compressed. We quantified the

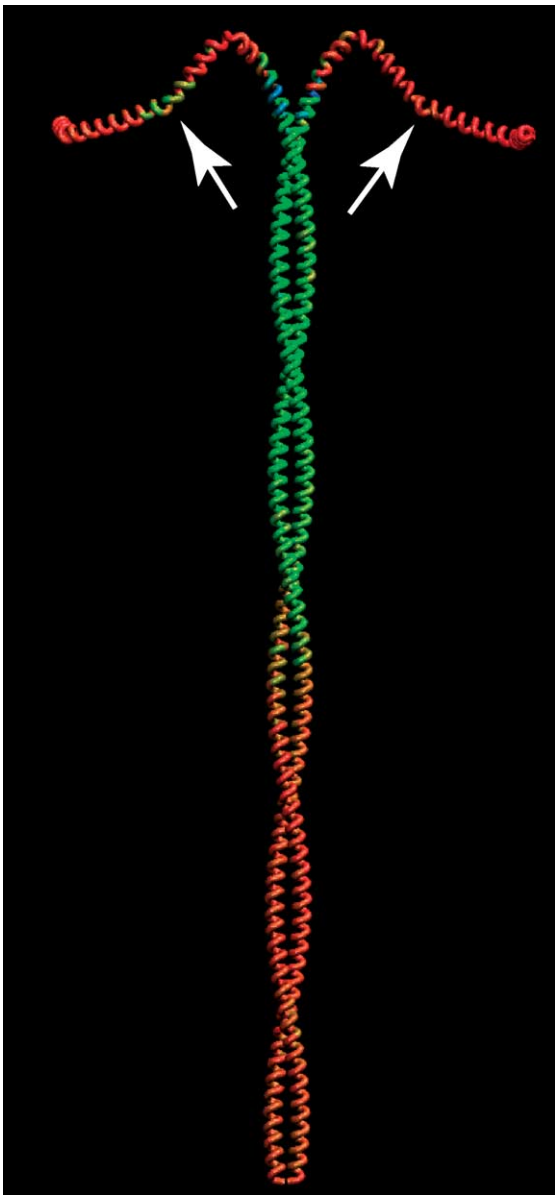

Figure 3. Bond strain in the smHMM heavy chain, color-coded from red (lowest) to blue (highest). An arrow denotes the stress point between the ELC and the RLC. The strain in the HC after the conformational change has been mapped onto the initial structure of the HC. The Figure is displayed using VMD.[93]

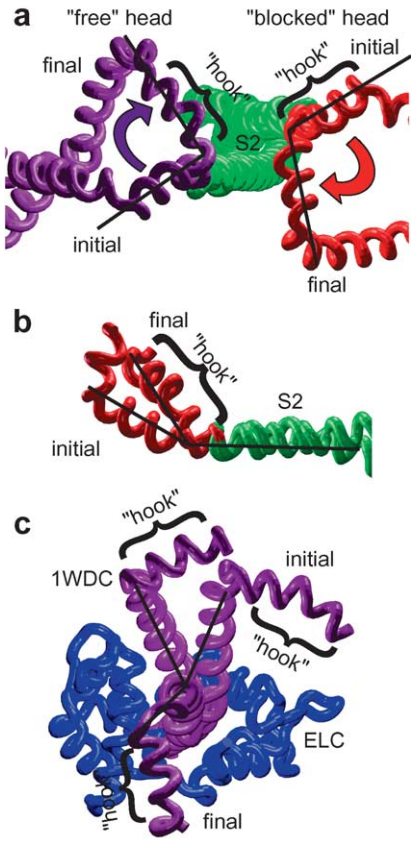

Figure 4. Key movements in the active to inhibited transformation. (a) This view shows the sense of the rotation about the two α-helices of S2. For clarity, S2 extends down, away from the observer. The hook domain corresponds to HC residues W840–Q852. Although the arrow indicates a clockwise rotation, with respect to the direction that S2 is extending (down, away from the observer) this is an anticlockwise rotation about the individual α-helices. This motion is unwinding with respect to the twist of the α-helix, because an anticlockwise (+) rotation at the beginning of the right-handed helix reduces its total twist. (b) View looking perpendicular to the S1–S2 junction showing the change in bending at this location between initial and final models. This view is for the blocked head but the bending for the free head is nearly identical. (c) View looking down the lever arm toward the ELC of the free head with the RLC removed for clarity and with the HC α-helix extending up toward the viewer. HCs from the two-heptad final model and the scallop myosin lever arm (PDB 1WDC) are aligned to this domain of the initial model. Movement from the initial model involves a bend and a clockwise rotation about the HC between the ELC and the RLC. This is also an unwinding motion, because a clockwise (−) rotation at the end of the α-helix (i.e. at the hook) reduces the total twist of the helix. Note that the 1WDC structure bends in the direction opposite to that of the active to inhibited conformational change.

secondary structure changes within the individual domains and the distribution of C^{α}–C^{α} distances for the entire model (Table 2). Models with the smallest changes were presumably the easiest to conform to the inhibited structure. These measures paralleled the strain energy calculated using equation (1) as shown in Table 1.[27]

For active-state models with the same number of atoms but that differ in the number of non-coiled heptads at the S1–S2 junction, the structural changes, in general, parallel the rms deviation between final model and inhibited structure. The final models that could be conformed closest to the inhibited structure, i.e. the two-heptad and three-heptad models, had the smallest overall changes in both S1 and S2. The zero-heptad model had slightly

Table 2. Dependence of structural distortions on S2 length

Model[a]	RMS deviation (Å)[a]	Δ Secondary structure[a]	Domain RMS deviation (Å)[a]	σ C^{α}–C^{α} (Å)[a]
Two-heptad$_{1105}$	6.3			
S1		0.120	2.05	0.133
S2 (852–931)		0.848		0.266
S2 (852–1105)		0.340		0.245
Two-heptad$_{931}$	6			
S1		0.167	2.37	0.145
S2 (852–931)		1.474		0.499
Two-heptad$_{931}$	10			
S1		0.118	2.16	0.119
S2 (852–931)		1.237		0.438
Two-heptad$_{1105}$	10			
S1		0.125	1.66	0.102
S2 (852–931)		0.303		0.251
S2 (852–1105)		0.131		0.212
Two-heptad$_{1940}$	10			
S1		0.070	1.32	0.098
S2 (852–931)		0.132		0.207
S2 (852–1105)		0.108		0.172
Rod (852–1940)		0.020		0.109

[a] Footnotes are as for Table 1.

smaller changes in S1 and the four-heptad model had slightly smaller changes in S2 but neither could be conformed correctly to the inhibited state structure.

Structural distortions were also compared between two-heptad active-state models with coiled coil lengths of 80, 254 and 1089 residues (whole myosin). Despite having more than four times the coiled coil length of the smHMM models, the full-length active myosin conforms well to the inhibited state structure with an rms deviation of 10 Å and with correct placement of the RLC and S2. To facilitate a quantitative comparison with whole myosin, models with shorter coiled coils were conformed to the same rms difference rather than the closest final state. The results indicate that the longer the length of coiled coil, the smaller the distortion introduced into both S1 and the coiled coil (Figure 5). The modelling suggests that flexibility in the coiled coil with respect to the conformational change to the inhibited state increases with the length of the coiled coil. The initial steep descent in the graph at short lengths of S2 and the shallow descent at long S2 lengths indicate that once a threshold is reached, further effects of the coiled coil length are small. This trend is similar to coiled coil length effects seen in kinesin processive movement.[28] The graph suggests that coiled coil length effects on cooperative movements need to be measured initially with the shortest possible coiled coil.

In all final smHMM models, the S2 structure departs significantly from the regular α-helical coiled coil of the starting model (Figure 6(a)–(e)). The regular pattern of crossovers spaced ~50 residues apart (Figure 6(a)) is reduced to an irregular pattern of 28–63 residues per crossover. The region closest to the S1–S2 junction (residues 852–931) changes more significantly. In the final

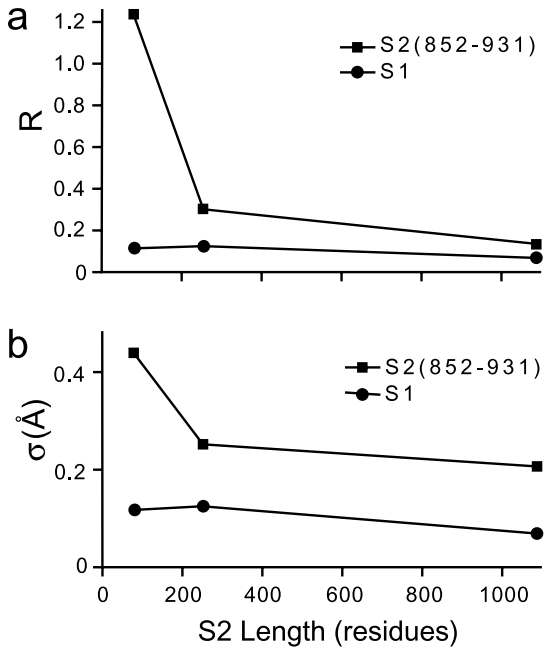

Figure 5. Effect of coiled coil length on the conformational transition for two-heptad models with varying amounts of coiled coil. (a) Change in secondary structure with coiled coil length; determined using MOLAUTO.[92] Change is calculated using $R = \Sigma|F_i - F_f|/\Sigma|F_i|$, where the summation is over four classes of secondary structure; coil, helix, sheet and turn. F_i and F_f are the fraction of the particular secondary structure in the initial and final models, respectively. (b) Change in standard deviation of C^{α}–C^{α} bond length with length of coiled coil. The average C^{α}–C^{α} distance stayed very uniform, between 3.8 Å and 3.9 Å. The value for the initial model was 3.85(±0.05) Å. (■). The first 80 residues of the S2 domain; (●) the S1 domain. The first point on the curve corresponds to an S2 length of unregulated smHMM, the second to a regulated smHMM and the last to whole myosin.

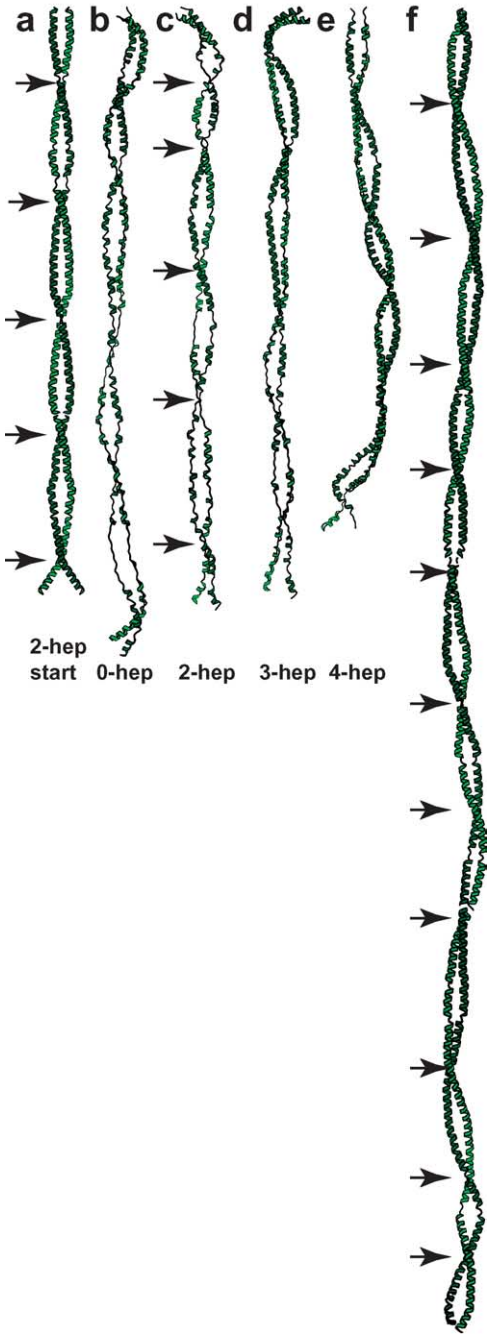

Figure 6. Effect of myosin head movements on S2 and LMM. (a) Starting S2 domain with two non-coiled heptads. Arrows denote crossovers at 50 residue intervals. (b–e) The zero, two, three and four-heptad S2 after conforming the starting models shown in Figure 1 to the inhibited state structure. The regular crossover spacings in the starting model become irregular and secondary structure changes in places from α-helix to coil. This results also in a lengthening of S2. Note that, despite all these changes, the total twist of the coiled coil exemplified by the number of crossovers remains constant. (f) Residues 1371–1940 of the myosin rod after NMA. Arrows indicate irregularly spaced, coiled coil crossovers. The Figure is displayed using MOLSCRIPT.[94]

whole myosin model, the structural changes were much smaller than those seen with the shorter coiled coil models. Nevertheless, even in whole myosin, the evenly spaced crossovers within the LMM coiled coil were changed to an irregular pattern (Figure 6(f)), suggesting that the stable head–head interaction in inhibited smooth muscle myosin propagates distortions through S2 into the LMM domain.

The changes in secondary structure in the S2 domain resulting from the conformational change to the inhibited state effectively lengthen the S2 as its α-helical content is reduced and its non-helical coil content rises (Figure 6(a)–(e)). This occurs without a large change in total twist of the coiled coil because the number of crossovers remains constant.

Discussion

Validation of the models

We have used a combination of homology modelling, experimental structures and elastic network NMA to examine the active to inhibited conformational change in smooth muscle myosin. Homology modelling was necessary because high-resolution crystal structures do not exist for all domains of smooth muscle S1 nor is a high-resolution structure available for the coiled-coil domain. A particularly important uncertainty is the structure of the RLC. None of the crystal structures for smooth muscle S1 contains the RLC and none of the complete S1 structures shows the N-terminal 24 residues that are involved in phosphorylation-based activation. The N-terminal 24 residues are probably not important for modelling the conformational change toward the inhibited state of smHMM because deletion of the first 16 residues of the smooth muscle RLC does not by itself activate the actin-activated ATPase.[25] Myosin with such an RLC cannot be activated, because a deletion of this size removes the myosin light chain kinase-binding domain. Presumably, deletion of the additional eight residues also would not lead to activation.

There are two crystal structures in the Protein Data Bank that contain coordinates for the RLC. The scallop regulatory domain structure was obtained in the presence of Ca^{2+} and would correspond to an activated myosin.[29] The chicken skeletal muscle structure most likely contains a non-phosphorylated RLC, as no effort was made to phosphorylate the myosin before crystallization.[30] The regulatory domain structures differ in two ways; the bend in the heavy chain between the ELC and the RLC and the bend in the hook. Wendt *et al*.[6] used the more bent structure from chicken skeletal muscle S1 in their inhibited state structure, so both homology models incorporated a similar bend in this location. The modelling shows that heavy chain bending between the ELC and RLC is important for the conformational change to the inhibited state. As

described further below, this could be an important clue to the structure of the phosphorylated regulatory domain in smooth muscle myosin. The orientation of the hook required separate RLC homology models. However, the importance of the hook orientation to the conformational change could not be determined from our modelling, because both RLC homology models produced similar results.

A second aspect of the model is the structure of the S2 domain. Until recently, there was no crystal structure of the S2 domain, but the structure of the first 51 residues of the S2 from scallop striated muscle myosin shows two heptads of unstable coiled α-helix after the S1–S2 junction.[22] This structure supports our modelling in two ways. First, it agrees with the starting model that conformed most accurately to the inhibited-state structure, which had two heptads of non-coiled α-helix after the S1–S2 junction. Second, it shows that the initial two heptads of S2 are α-helical.

In our models for S2, we tested only four possible lengths of non-coiled α-helix after the S1–S2 junction. The results showed two important mechanical characteristics. If the coiled coil begins too close to the S1–S2 junction, it prevents the S1 heads from moving independently and if it occurs too far away, the coupled motion is disrupted. The experimental data upon which the models were based used a leucine zipper to define the initiation of coiling.[8] Strong triggering sequences can propagate coiled coil over long distances.[31] Nevertheless, a zipper sequence after two heptads of peptide cannot propagate very far before it would disrupt regulation. More relevant perhaps is the question of how far a zipper sequence can propagate coiled coil when placed after seven heptads of peptide. Our modelling would suggest that it would need to propagate four or five heptads in order to restore regulation. The initial 15 heptads of the smooth muscle myosin S2 does not form a strong coiled coil by itself,[8,32] requiring a trigger sequence further down the coiled-coil domain for stability.[31] The key structural feature suggested by the modelling is that the heads must be capable of moving independently but without so much flexibility that coupled motions are disrupted.

In constructing the model for the complete myosin rod, we assumed the structure was entirely coiled coil, even though assessments using PAIRCOIL and COILS indicated several regions of poor coiled coil potential. The atomic structures of these regions are unknown but protein secondary structure predictions do not suggest any β-strand; predictions indicate either α-helix or undefined, which we assume indicates random coil. Poor coiled coil potential does not necessarily equate to poor helix-forming potential, because the coiled coil is defined by particular matches between hydrophobic and charged residues in the adjacent helices.[33] The structure of random coil peptide is undefined and therefore difficult to model. Our modelling with β-strand placed after the S1–S2 junction indicates that this would cause uncoupling of torsional motions. However, the rest of the modelling suggests that non-helical coil itself does not. As the initial α-helical S2 and rod models are conformed to the inhibited state, the helix content drops and non-helical coil content increases, yet the coupling is unbroken.

We chose to build a theoretical model for the active state of smHMM because the available experimental structural information for phosphorylated smHMM was inadequate. In the activated state, it is known from electron microscopy observations that the two heads of smHMM are not interacting yet adopt a wide range of positions with respect to the S2 domain.[11,13,34] These positions presumably represent random motions of the individual S1 heads that are not necessarily steps in the conformational change to the inhibited state. The key feature of the activated state is the lack of association between the myosin heads other than at the beginning of the coiled coil. As shown by our modelling, torsional motions of the myosin heads can lead to distortions of the coiled-coil domain. The lowest energy state of the coiled coil is therefore likely to be at or near the symmetrical arrangement depicted by our putative active-state models.

The N-terminal residues of the RLC beginning at M24 are highly mobile, as shown by NMR studies.[35] If these N-terminal residues occupied a fixed position on the myosin lever arm in the dephosphorylated state they could affect the modelling results, depending on their actual structure and interactions. However, such a fixed interaction has not been demonstrated. If after dephosphorylation, the initial step towards the inhibited state, these residues become disordered, as suggested by the lack of any density from this feature in any of the myosin S1 crystal structures that possess this portion of the RLC,[29,30] they would not affect the modelling results.

On the basis of the above, we believe that our initial models are consistent with experimental observations and are adequate representations of the smHMM and myosin structures at the beginning of the conformational change toward the inhibited state.

Coupling between myosin heads and the S2 domain

The key observation from our modelling of the active to inhibited transformation in smHMM is the interdependence of the head–head interaction and the S2 domain. The models of whole smooth muscle myosin suggest that the head–head interaction propagates throughout the coiled-coil domain. These effects are due to the torsional motions of the myosin heads as they move from opposite sides of S2 toward the same side, and their propagation throughout the coiled coil is apparently due to the high α-helical content of the myosin rod. Myosin is unusual among proteins, in that it has extremely

long α-helices within the rod domain, which may give myosin unusual properties.

Our modelling suggests that coupled torsional motions of the myosin heads affect the structure of the coiled-coil domain and, conversely, that the structure of the coiled-coil domain, in particular its length, affects the coupled motions of the myosin heads. The concept of coupled motions between the myosin heads and the coiled-coil domain may explain and integrate many experimental observations on myosin function.

Two key functional characteristics of smooth muscle myosin can be explained by the coupled motions between myosin head and the coiled-coil domain. First, it is widely known experimentally that MgATP added to a suspension of dephosphorylated smooth muscle or non-muscle myosin filaments results in their immediate dissolution.[15] ATP is necessary for this change to produce the S1 conformation found in the inhibited state.[36] Mechanisms to explain this have generally suggested that ATP binding shifts the equilibrium between monomer and filament toward monomer.[37,38] Our modelling provides a structural basis for this equilibrium shift. Filament formation primarily involves the LMM domain, which begins ~40 nm from the myosin heads. Our studies show that distortions introduced into the coiled coil as the S1 heads conform from the active to the inhibited structure are propagated along the entire myosin rod. This distortion produced in a large number of myosin molecules could destabilize the filament, since the tight packing of LMM possible with a regular coiled coil is disrupted. As the myosin is released from the filaments, further folding into the 10 S conformation occurs until all the myosin is dissolved. This scenario is consistent with measurements that show ATP binding and cleavage, both of which must occur before the head–head interaction is possible, are fast compared to filament dissolution.[36]

Second, biochemistry suggests that both dimerization through the coiled coil and a minimal length of coiled coil are requirements for smooth muscle myosin regulation.[8,9,10,39] Dimerization can be achieved with only a leucine zipper sequence (32 residues) after the S1–S2 junction. However, such constructs are not regulated. Our models demonstrate how the length of the coiled coil affects this transition. During the active to inhibited conformational change, each S1 head acts as a lever to introduce torque into its HC component of S2. The response of each α-helix in S2 to this torque depends on its torsional flexibility. In homogeneous rods, torsional flexibility is linearly proportional to length.[40] Thus, the length of the coiled coil, more importantly, the length of its α-helices, facilitates the transition by distributing the distortions introduced by the S1 head movements over more atoms.

Recent observations on the structure of monomeric smooth muscle myosin using atomic-force microscopy observed a lengthening of the rod domain and a shift further from the S1–S2 junction of predicted bends in the rod domain.[34] The second bend was pushed further from the junction than the first bend. Our modelling shows that the stable head–head interaction of inhibited smooth muscle myosin propagates distortions into the entire coiled coil that reduce the α-helix content and raise the non-helical coil content (Figure 6). The resulting rod lengthening would tend to push identifiable features of the coiled coil further from the S1–S2 junction. The greater effect would occur for features more removed from the S1–S2 junction. At the same time, this could amplify weaknesses in the coiled coil, thereby introducing bends not observed in the activated state. The effect of the head motions may not be entirely limited to the inhibited-state conformation of smooth muscle myosin. Any torsional motion of the heads about their S2 α-helices could propagate through the rod domain. In this regard, it is significant that in smooth muscle myosin rod, a structure lacking the S1 heads entirely, only a single bend is seen, which corresponds in location to the first region of low coiled coil probability.[41]

Deletion of the first 16 residues of the smooth muscle myosin RLC (NDL-16) leads to a myosin with altered viscosity, raised MgATPase activity, but with low actin-activated ATPase activity.[25] An RLC truncated to this extent cannot be phosphorylated by myosin light chain kinase, but the deletion by itself does not lead to activation. NDL-16 myosin cannot form the 10 S structure, yet the viscosity of this myosin in 0.15 M KCl is similar to that of 6 S myosin in 0.4 M KCl, suggesting that it remains monomeric. Its altered properties, in particular low actin-activated ATPase activity, suggest that the two S1 heads are in the inhibited-state conformation. Incorporation of NDL-16 myosin into filaments at low ionic strength increases its ATPase activity, with and without actin, but well below levels typical for phosphorylated myosin at the same ionic strength. Our modelling suggests that its altered viscosity is due to distortions in the myosin rod that inhibit filament formation at physiological ionic strength. The raised ATPase activity when incorporated into filaments at low ionic strength may be explicable by other effects, as described below.

If the coupled motion to achieve the inhibited state of smooth muscle myosin can propagate distortions along the myosin rod, thereby altering thick filament stability, it follows that conditions, such as low ionic strength and high concentrations of Mg^{2+} that increase thick filament stability by tightening interactions between the rod domains, may affect the ability of the two myosin heads to achieve the inhibited state. This inference may underlie some apparently contradictory results on activation of filamentous smooth and non-muscle myosin by RLC phosphorylation.

Relationship of head–rod coupling to ATPase activation

ATPase activation by RLC phosphorylation in

filamentous smooth muscle myosin at physiological ionic strength has been demonstrated using conditions in which the filaments were stabilized by antibodies to the myosin rod.[42] Under these conditions, a 30–100-fold increase in actin-activated ATPase rate was observed. This result is in contrast to studies of smooth muscle and non-muscle myosin regulation, where the filaments were stabilized by high concentrations of Mg^{2+} and low ionic strength.[43–46] With filaments formed at low ionic strength, the ATPase activity was relatively high in the dephosphorylated state and showed only a small increase on phosphorylation. The major effect of phosphorylation seemed to be an increase in actin binding. This apparent contradiction may be explained by coupled motions of myosin heads with myosin rod.

One of the main factors affecting filament formation is the regular pattern of charged residues along the myosin rod, the pairing of which determines the spacings along the thick filament.[26,47] Our modelling shows that the head–head interaction can disrupt regular patterns within the coiled coil myosin rod. Conversely, strengthening the regular pattern of charged interactions in the myosin rod, with low ionic strength and high concentrations of Mg^{2+}, will inhibit the head–head interaction and may also "zip up" the S2 domain into the filament backbone. Inhibiting the head–head interactions increases the number of free myosin heads available for interacting with actin, thereby raising the actin-activated ATPase activity of the non-phosphorylated myosin.

If tight packing of the myosin rod into a filament backbone disrupts the head–head interaction thereby elevating the ATPase activity in the dephosphorylated state, how then is the actin binding increased by phosphorylation? Presumably, free myosin heads in any form are equally free to bind actin. Packing the myosin into filaments frees the RLC N terminus from its involvement in stabilizing the 10 S conformation. The RLC N terminus is highly positively charged, whereas the rod domain has an overall negative charge, with repeating clusters of positive and negative charges.[26] Intramolecular binding to free myosin rod and intermolecular binding to filamentous myosin rod are not so very different. An interaction between the N terminus of the RLC and the filament backbone might inhibit movements of the myosin heads toward actin, while RLC phosphorylation inhibits that interaction, thereby raising the myosin–actin affinity. The possibility that similar interactions between the RLC and the rod domain might occur in both 10 S and filamentous myosin was suggested some years ago.[48]

The MgATPase rate of the 10 S conformation is exceedingly slow, suggesting that the folded conformation traps the hydrolysis products extremely well.[36,37,42] Incorporation of unphosphorylated myosin into filaments increases the ATPase rate by a factor of at least 10 and sometimes by as much as 100-fold, depending on experimental conditions. Myosin in the 6 S conformation, which lacks the head–head interaction found in the 10 S conformation, has an even faster MgATPase, whether phosphorylated or not. This product release is not the actin-stimulated release, which is fast, but rather the release of hydrolysis products by myosin itself, which is very slow. Sellers hypothesized that it was the rate of product release that was stabilized in dephosphorylated smooth muscle myosin,[4] and a mechanism was suggested by the intramolecular head–head interaction found in dephosphorylated smHMM.[6] In the 10 S conformation, the bending of the rod domain, which we hypothesize is due to head–rod coupling, is stabilized by the N terminus of the RLC.[25] Through coupling between heads and rod, anything that stabilizes the bent hairpin conformation of the rod will in turn stabilize the head–head interaction that inhibits phosphate release. Incorporating myosin into filaments will disrupt this stabilization. In this case, interactions between the RLC N terminus and the filament backbone may not be able to stabilize the head–head interaction and, if it does, must do so by a different mechanism than that used in the 10 S conformation.

ATPase activation by RLC phosphorylation

The conformational change to bring the two widely separated heads in the active state to the inhibited conformation involves a number of movements about points of flexibility. The largest changes are seen at the S1–S2 junction, where both heads use an anticlockwise twist about their S2 α-helices to bring both heads into contact. The sense of the motion is in a direction to unwind the S2 α-helices (see the legend to Figure 4), a process that may make the S1–S2 junction more flexible to the bending motion that occurs also at this location.

An unusual feature of the conformational change is the common direction of twist about the S2 α-helices of both heads. This seems almost counterintuitive, analogous to a "dog chasing its tail". However, the two heads are not twisting about the S2 axis, but are twisting independently about their own S2 helices. The motion brings the two motor domains closer to each other and to S2. The amount of twist is similar to removing an amino acid residue from each HC at the S1–S2 junction. This could be tested experimentally, as it predicts a way to improve regulation in short S2 constructs with impaired regulation. A related experiment has been published, but with constructs that were much longer than the minimum needed for regulation.[39]

Another important movement occurs in the HC between the ELC and the RLC. This particular region is at the Ca^{2+}-binding site on the lever arm in scallop myosin,[29] which, by analogy with RLC phosphorylation in smooth muscle myosin, activates the actin-activated ATPase. Negative stain and rotary shadow electron microscopy have shown that scallop HMM forms a structure very similar to smooth muscle HMM,[18,49] suggesting

that the mechanisms are related. In scallop HMM, Ca^{2+} coordinates with the ELC, thereby promoting an interaction with the RLC that is thought to stiffen the lever arm against any HC bending needed to achieve the inhibited state.[29] When the scallop lever arm structure is aligned with the ELC in the active-state model, the direction of bending between the ELC and RLC is opposite to that needed to go from the active to the inhibited-state structure (Figure 4(c)). This would suggest that phosphorylation of S19 on the RLC might position the N-terminal residues to straighten the smooth muscle lever, as is found in the scallop regulatory domain. Both Ca^{2+} in scallop myosin and the N terminus of the smHMM RLC would thus stabilize the structure against the motion shown here that is needed to form the inhibited-state conformation.

Head–rod coupling in myosin filaments

The coupling between S1 head movements and the coiled-coil domain demonstrated by our modelling may integrate a large number of experimental observations on myosin filament structure. An important but unanswered question is the conformation of dephosphorylated myosin in smooth muscle thick filaments. This has been difficult to resolve, due to the solubility issue. However, the coupling between myosin heads and the coiled-coil domain demonstrated by our modelling may have relevance to thick filament structure in general and, in particular, the nature of the interactions between myosin heads.

The 10 S conformation has been most studied in smooth and non-muscle myosin. However, it has been observed *in vitro* using scallop striated muscle myosin[17] as well as cardiac and skeletal muscle myosin.[50] This suggests that intramolecular head–head interactions are an inherent property of myosin II, even in "unregulated" myosin. However, the ease with which the 10 S conformation forms may differ among isoforms and may be related to head–head interactions in relaxed thick filaments. In addition, evidence that both intramolecular and intermolecular interactions of similar form can occur between myosin heads in different states is provided by 2-D arrays of smHMM formed both with and without RLC phosphorylation.[14] Similar head–head interactions were seen in both states but differed mainly in whether they were inter- or intramolecular in nature.

In contrast to smooth muscle myosin, several structures of relaxed striated muscle myosin filaments have been determined.[51–56] Striated muscle thick filaments are bipolar, with a central bare zone and two helical regions on either side. Many of the 3-D images of these filaments show the myosin heads splayed apart to lie along long-pitch helical tracks in such a way that individual heads from successive repeats of the 14.3 nm period interact.[52–56] In some cases the resolution is not sufficient to clearly distinguish intramolecular from intermolecular head–head interactions, but in other cases the interpretation is very clear. Relaxed thick filaments from insect flight muscle follow a similar principle, except that the interaction between myosin heads from adjacent molecules occurs within the individual 14.5 nm repeats.[51] These intermolecular head–head interactions serve to sequester myosin heads against the thick filament backbone and away from actin.

Smooth muscle thick filaments, on the other hand, are not helical and have a side polar arrangement when formed *in vitro* under some conditions,[37,57,58] but also when observed *in situ*.[59] These filaments have a square cross-section with the myosin heads on two of the opposing sides polarized oppositely. Their apparent lack of a helical structure may inhibit intermolecular head–head interactions in the relaxed filament.

As a conformation for sequestering myosin heads in thick filaments from actin, the inhibited structure observed by Wendt *et al*.[6] has some attractive features. The conformation occupies the actin-binding domain of the blocked head through interaction with the free head, and directs the actin-binding domain of the free head away from neighboring actin filaments and toward the thick filament backbone. It could therefore accomplish the same sequestering function in the relaxed state as the intermolecular interaction seen in bipolar thick filaments, but using a different structure.

Although different species of myosin may differ in detail, we suggest that head–head interactions in whatever form, inter- or intramolecular, are a general feature of relaxed thick filament structure. Features of the rod domain packing, among others, may determine which kind of interaction predominates. Our modelling suggests that one factor affecting intra- or intermolecular head–head interactions is the length of S2 or, more precisely, the portion of S2 that is free of the thick filament backbone. In smooth muscle myosin, S2 length is a key determinant of the actin-activated ATPase regulation.[8] However, the actual length of S2 that is free of packing constraints within the thick filament backbone is not well defined. The length of S2 is defined by proteolysis of monomeric myosin in high salt; the cleavage site is inaccessible in filaments leaving open the question of how much S2 is free of the filament backbone. To our knowledge, the only work that has actually measured the length of S2 *in situ* when actin and myosin are interacting shows a length of seven to ten heptads.[60] This may be too short for regulation in smooth muscle myosin, which needs at least 140 residues of S2 or about twice what has been seen *in situ* in muscle. Some evidence that the amount of free S2 in smooth muscle thick filaments may be longer than seven to ten heptads can be found in the extreme distances that myosin heads have been observed to extend from the thick filament backbone.[61]

A preference for intermolecular head–head interactions seen in most striated muscle thick filaments over intramolecular interactions possible in isolated myosin may arise from differences in the packing of

the rod domain within the filament backbone. If the packing is tight and involves a significant portion of the S2 domain, then the amount of free S2 will be small and inhibiting for an intramolecular interaction. The intermolecular interaction would then be favoured, because the myosin heads can remain on opposite sides of S2 and large torsional motions are not needed to facilitate head–head interactions.

If the rod packing involves less of the S2 domain, intramolecular head–head interactions may be favoured, thereby facilitating some functions at the potential cost of filament instability. Filament instability in the inactive (relaxed) state may be functionally advantageous for non-muscle myosin, but probably not for muscle myosin. *In vivo* in all muscles, even smooth muscle, the filaments are stable under relaxing conditions.[62] If an intramolecular interaction between myosin heads occurs in relaxed smooth muscle filaments, then some factor would be needed to stabilize the filaments. The myosin concentration in all muscles is much higher than typically used *in vitro*, which would shift the equilibrium toward filament formation.[38] While this may be true, it would result in high turnover within the filaments and constant reassembly of the contractile apparatus. However, smooth muscle thick filaments contain the proteins caldesmon[63] and telokin,[64] both of which are known to stabilize thick filaments and could thereby stabilize the contractile apparatus.

If filament instability is the consequence of the relaxed conformation in smooth muscle myosin, there should be a compensating functional advantage. The side polar arrangement of smooth muscle myosin filaments permits more myosin head attachment to actin than would be possible in bipolar thick filaments of the same length and a higher force per thick filament for the same amount of myosin. It allows also for greater muscle shortening, as actin filaments are less likely to encounter oppositely polarized actin molecules coming from the other direction.[59] However, another possibility might be to facilitate head–head interactions in single-headed actin attachments or two-headed attachments to actin filaments in contracting muscle. The former are suggested by actin binding of dephosphorylated smHMM,[7] but this interaction has not been characterized extensively. In contrast, there is abundant evidence for two-headed actin filament attachments.

Implications for function in two-headed motors

The motion described here is an independent twisting of individual α-helices in the S2 domain, which brings the two S1 heads closer together to form the inhibited state. Functionally related motions may occur in other myosin II states and in other motors that form dimers through an α-helical coiled coil. One such function is the simultaneous formation of bonds between actin and myosin in muscle. This requires two myosin heads initially on opposite sides of S2 to come to the same side in order to bind actin. In rigor muscle, two-headed binding to actin predominates,[60] and because of the high actin–myosin affinity, is even unaffected by the length of the coiled coil.[65] However, in contracting muscle, single-headed binding to actin is the norm.[66,67] In addition, single-headed myosin functions as well as two-headed myosin in a number of studies that have measured motility, ATPase activities and tension development.[68,69] This suggests limitations to two-headed interactions where one head may be bound weakly. Our modelling suggests that these limitations arise from torsional rigidity of the S2 α-helices.

On the other hand, *in vitro* experiments with smooth muscle myosin have suggested that the two myosin heads can bind actin simultaneously to obtain optimal mechanical performance,[70] even when one is inactive.[71] Other biochemical studies have detected cooperativity in kinetic steps of rabbit skeletal muscle myosin binding to actin.[72] However, these experiments were done using S2 constructs ~46 heptads long, which are much longer than its length observed *in situ*.[60] These apparently conflicting observations may be reconciled by a variable length of free S2; in some myosin filaments, such as those from striated muscle, the free length of S2 may be short and inhibiting for two-headed interactions with actin, whereas in others, such as smooth muscle, it may be much longer and not inhibiting. We suggest that in HMM molecules with long S2 domains, the myosin heads have more torsional flexibility to twisting about their S2 α-helices than they would if incorporated into filaments. This interpretation is testable using HMM constructs with short S2 domains.

In processive motors such as kinesin and myosin V, at some point in the ATPase cycle, both heads must be bound simultaneously to their filament track.[73] Because these tracks are polar, this would involve a movement in which the detached motors initially face away from each other on opposite sides of the coiled coil, to facing in the same direction when bound. It is commonly thought that processive movement using a hand-over-hand mechanism involves alternating twisting motions of 180° about the coiled coil.[74] However, by analogy to the motion modelled here for smooth muscle myosin, this might instead be accomplished by twisting motions about the individual α-helices of the coiled-coil domain. It is pertinent that myosin V isoforms from yeast are non-processive motors with a relatively low duty cycle compared with other myosin V isoforms.[75] They also have the shortest coiled coil of any of the myosin V isoforms, even shorter than that used in most expressed recombinant myosin V isoforms.[76]

Recent studies of processive motion in kinesin have observed an effect, described as limping, that is a function of the length of the coiled coil.[28] Limping is an alternation of steps with short and long dwell times; the long duration steps were found to be sensitive to the length of the coiled coil.

This was interpreted as due to chirality in the torsional flexibility of the coiled coil, but might be explicable by chirality in the torsional flexibility of the individual α-helices such that the ease of an unwinding twist is greater than the ease of a winding twist. In the present study, all the large torsional movements are in a direction to unwind the α-helix. If only large unwinding twists are allowed, it could mean that the motions of the two heads are topologically different, with one head twisting inwards toward the coiled coil (and the microtubule track) in one step and the other twisting outward away from the coiled coil in the alternating step. Alternatively, if one head twists clockwise the other would twist anticlockwise. The torsional rigidity of the α-helix may be quite sensitive to the sense of the twist.

Conclusion

Our studies combined experimental information, homology modelling and elastic network NMA to explore the effect of S2 structure on the rearrangement of the two smooth muscle myosin heads during the active to inhibited transition. The results point to the importance of torsional flexibility of the α-helices within the S2 domain as an important factor in modulating myosin function. The modelling suggests that a flexible hinge is not necessary between the myosin head and the S2 domain, the α-helix has enough flexibility provided it is sufficiently long. Moreover, an α-helical S2 domain facilitates coupled motions between S1 and S2, which can be communicated along the entire length of the rod.

Modelling Methods

S1 and RLC domains

We built putative active-state models for smooth muscle myosin and smHMM using homology modelling, structural data from known crystal structures, and experimental constraints, i.e. the active state has S1 heads spaced widely on opposite sides of S2,[11,13] and the S2 domain is an α-helical coiled coil.[26]

The structure of ATP-bound smooth muscle S1 consisted of the motor domain-ELC fragment structure (PDB 1BR1)[77] and a homology model for the RLC and its bound segment of HC. Homology models were built for the two possible structures of the RLC-HC domain, one based on the scallop myosin regulatory domain, PDB 1WDC,[29] the other based on chicken skeletal muscle S1, PDB 2MYS.[30] All of the work reported here is from the model based on the 2MYS template. The homology model based on PDB 2MYS used RLC coordinates with side-chains built in, which was kindly provided by Dr Ivan Rayment. The smooth muscle myosin HC sequence was taken from SwissProt MYHB_CHICK, and the smooth muscle RLC sequence from SwissProt MLRM_CHICK. None of the experimental structures for the RLC shows the N-terminal 24 residues involved in phosphorylation. These were, therefore, left out in our modelling.

The RLC sequences were aligned using the multiple sequence alignment feature of GCG.[78] We used all of the RLC sequences that could be found in the Protein Data Base for this alignment. After sequence alignment, peptide segments of the same length were modelled by first building a lattice-based SICHO model,[79] and then incorporating the correct side-chain. Only the residues that differed from the template were changed by this procedure. Loops that varied in length between the smooth muscle isoform and the template RLCs were modelled separately, using a replica exchange lattice modelling protocol.[80] The heavy chain segment, residues 793–852 were built in a similar fashion, except that there were no loops to model. The RLC-HC model was then subjected to 100 cycles of steepest descent energy minimization using an *r*-dependent dielectric constant of 4.0 ($\varepsilon = 4.0\ r_{ij}$). This was followed by 1000 cycles of adaptive basis Newton–Raphson, using an implicit solvent generalized Born model.[81] After splicing on the RLC, the S1 model was subjected to 400 cycles of adaptive basis Newton–Raphson. All calculations were carried out using the MMTSB Tool Set.[80]

S1 was then aligned to the S2 model using residues V847–L851. Splicing of S2 onto S1 was done so that the heavy chain coordinates up to L851 were always taken from the S1 model. Residues Q852–L1105 were taken from the S2 model. Although Q852 is present in the homology model based on PDB 2MYS, it is distinctly non-helical. We replaced it with coordinates from the idealized α-helix to allow a more uniform continuation of the HC α-helix.

The RLC homology model based on the scallop regulatory domain structure (PDB 1WDC) differs from the model based on the chicken skeletal muscle RLC (PDB 2MYS) in the bend in the heavy chain α-helix between the ELC and the RLC and in the RLC structure itself, which changes the orientation of heavy chain residues 840–851 at the S1–S2 junction by ~15°. In both models, the heavy chain bend between the ELC and RLC was kept as found in 2MYS. However, both homology models produced similar results.

Model for the inhibited state of S1

For the inhibited structure, we used a crystallographically refined structure based on the results reported by Wendt *et al*. (PDB 1I84)[6,12] but which contained an homology model for the RLC domain (Figure 1(b)). This provided coordinates based on the smooth muscle sequence that were based on a quantitative fit rather than the visual fit used earlier. Although the Wendt *et al*. structure contains coordinates for the S2 domain, we used only the S1 coordinates in our inhibited state model. In the Wendt *et al*. model, only a small segment of density exhibiting a left-handed twist can be assigned reliably to S2 ($S2_{III}$). Two other segments ($S2_I$ and $S2_{II}$) were built by conjecture to connect $S2_{III}$ to the C terminus of the S1 domains. By excluding S2 from the inhibited-state structure, we could computationally test this conjecture.

The S2 domain

We chose to build our model for the activated state of smHMM by combining the S1 model derived above with a theoretical coiled-coil S2 domain. Previously, a model for the activated state had been proposed on the basis of electron micrographs of 2-D arrays of thiophosphorylated smHMM.[14] However, that model was based on projections alone of negatively stained specimens, did not include the S2 domain and had a hybrid structure for the

light chain binding domain consisting of the HC-ELC domain from chicken smooth muscle and HC-RLC domain from chicken skeletal muscle. We therefore considered a theoretical model for the activated smHMM to be more useful for the present study.

The S2 domain was modelled after its predicted α-helical coiled coil structure,[26] using a program supplied by Dr Gerald Offer.[82] The least understood part of the structure is the S1–S2 junction. Four models were made of the S1–S2 junction that had zero, two, three or four heptads of non-coiled α-helix after the S1–S2 junction. To determine the first or *a* residue for the coiled coil, we analyzed the S2 sequence of chicken skeletal, scallop striated adductor and chicken smooth muscle using the programs PAIRCOIL[83] and COILS.[84] Both predicted that the first *a* residue after the invariant proline residue, P849, was V853. For the two-heptad, three heptad and four-heptad smHMM models, a straight helix beginning at F844 was calculated from standard ϕ,ψ values using CHARMM.[85] Three extra residues were added to this helix at its C terminus to facilitate alignment with S1 and the coiled coil.

In the smHMM and myosin model, the HC length extends to residue 1105 and residue 1940. respectively. Except for the first two heptads after the S1–S2 junction, the rod domain (S2 plus LMM) for the whole myosin model was built as a continuous α-helical coiled coil. Coiled coil analysis of the myosin rod domain predicted three regions of low coiled coil probability, the first centered at residue L1185, the second at E1466 and a third at D1585. To determine a probable secondary structure for these regions, the myosin rod sequence was analyzed using several secondary structure utilities, the Predict Protein Server†,[86] and NNPREDICT‡.[87] None of the servers predicted any β-strand within these regions or any other region of the rod domain, except for residues beyond P1940, which was the last residue used in the modelling. The NNPREDICT server suggested 22% β-strand but only if the structure class was declared to be β-strand. All other cases predicted either α-helix or unassignable secondary structure, which we take to be non-helical coil. Under these circumstances, it was simplest to model the entire rod as a coiled coil. By virtue of the 2-fold symmetry of the coiled coil, all starting smHMM and myosin models have 2-fold symmetry.

Normally, we did not minimize the S2 domain because only the C^{α} coordinates were used to construct the elastic network model for subsequent normal mode analysis (NMA). To determine whether this was important, the two-heptad S2 model was minimized and the NMA repeated. The result was the same as when the minimized structure was used.

Normal mode analysis

The structural and mechanical requirements to conform a molecular structure between two functionally important states can be deduced from a simplified mechanical description of its molecular framework using NMA.[20,88] We used an elastic network model[89,90] to define the structure and connectivity of the atomic models for myosin described above:

$$E_P = \sum_{a,b} \frac{C}{2} (|\mathbf{r}_{a,b}| - |\mathbf{r}^0_{a,b}|)^2 \quad (1)$$

where $|\mathbf{r}_{a,b}| = |\mathbf{r}_a - \mathbf{r}_b|$ denotes the length of the vector connecting atoms a and b, and the superscript zero indicates the given initial configuration. The strength of the potential C is a constant that is assumed to be the same for all interacting pairs. The sum is restricted to atom pairs separated by less than $R_c = 10$ Å. In addition, only the C^{α} atoms were used,[20,90] and the RTB method was used to further reduce the computational costs.[88] The normal modes calculated on the basis of these elastic network models define the energetically preferred directions of deformation of the system. The lowest-frequency/highest-amplitude modes obtained with this elastic network NMA have been shown to be in good agreement with functionally important motions in biological molecules.[20,88]

Iterative exploration of large conformational changes

Since conformational changes are non-linear, the very large rearrangements needed to move from the active state of smHMM to its inhibited state cannot be generated from a single set of normal modes in a single iteration. Instead, an iterative approach is utilized to describe the conformational change.[27,91] The conformational change is described by the following procedure: the initial conformation is defined as $C_i = C_0$ and the final state is C_f. Normal mode analysis is performed on C_k. The vector difference $\Delta\mathbf{r}^k$ between C_k and C_f is re-evaluated. The structure C_k is displaced along a linear combination of normal modes $\mathbf{a}^k$ toward the final state leading to the structure S_{k+1}. The amplitude A_j^k of the displacement along a normal mode j is given by:

$$A_j^k = \mathbf{a}_j \cdot \Delta\mathbf{r}^k Q \quad (2)$$

where Q modulates the magnitude of displacement along the projection of mode j onto the current vector $\Delta\mathbf{r}^k$. In our calculations Q was chosen to be relatively small, $Q = 0.025$, and approximately 400 iterations were used to move from the initial to the final state.

Overlap

To measure how a given normal mode, $\mathbf{a}_j$, compares with an experimentally known conformational change, $\Delta\mathbf{r} = \mathbf{r}_1 - \mathbf{r}_2$, the overlap between the two vectors is calculated as:

$$I_j = \mathbf{a}_j \cdot \frac{\Delta\mathbf{r}}{|\Delta\mathbf{r}|} \quad (3)$$

An overlap of 1 means a given normal mode is in exactly the same direction as the conformational change, $\Delta\mathbf{r}$. In the present calculations, no information was used for S2 in the target, inhibited-state structure. Thus, the overlap was calculated only between the S1 domains, and the position of S2 is derived solely from the coupling between modes of S1 and S2.

Acknowledgements

We thank Drs Kathy Trybus, David DeRosier, Donald L. D. Caspar and Mary Reedy for their

† http://cubic.bioc.columbia.edu/predictprotein/

‡ http://www.cmpharm.ucsf.edu/(nomi/nnpredict.html

comments on early versions of the manuscript. Financial support from the NIH and the Center for Multiscale Modelling Tools for Structural Biology (RR12255, to C.L.B. III) and NIAMSD (AR47421, to K.A.T.) is greatly appreciated.

References

1. Sellers, J. R. (1999). *Myosins* (2nd edit.), Oxford University Press, New York, NY.
2. Holmes, K. C. & Geeves, M. A. (2000). The structural basis of muscle contraction. *Phil. Trans. Roy. Soc. ser. B*, **355**, 419–431.
3. Sellers, J. R. (1991). Regulation of cytoplasmic and smooth muscle myosin. *Curr. Opin. Cell Biol.* **3**, 98–104.
4. Sellers, J. (1985). Mechanism of the phosphorylation-dependent regulation of smooth muscle heavy meromyosin. *J. Biol. Chem.* **260**, 15815–15819.
5. Cremo, C. R., Sellers, J. R. & Facemyer, K. C. (1995). Two heads are required for phosphorylation-dependent regulation of smooth muscle myosin. *J. Biol. Chem.* **270**, 2171–2175.
6. Wendt, T., Taylor, D., Trybus, K. M. & Taylor, K. (2001). Three-dimensional image reconstruction of dephosphorylated smooth muscle heavy meromyosin reveals asymmetry in the interaction between myosin heads and placement of subfragment 2. *Proc. Natl Acad. Sci. USA*, **98**, 4361–4366.
7. Sellers, J. R., Eisenberg, E. & Adelstein, R. S. (1982). The binding of smooth muscle heavy meromyosin to actin in the presence of ATP. Effect of phosphorylation. *J. Biol. Chem.* **257**, 13880–13883.
8. Trybus, K. M., Freyzon, Y., Faust, L. Z. & Sweeney, H. L. (1997). Spare the rod, spoil the regulation: necessity for a myosin rod. *Proc. Natl Acad. Sci. USA*, **94**, 48–52.
9. Rosenfeld, S. S., Xing, J., Cheung, H. C., Brown, F., Kar, S. & Sweeney, H. L. (1998). Structural and kinetic studies of phosphorylation-dependent regulation in smooth muscle myosin. *J. Biol. Chem.* **273**, 28682–28690.
10. Ikebe, M., Yamada, M., Mabuchi, K., Kambara, T. & Ikebe, R. (1998). A specific amino acid sequence at the head–rod junction is not critical for the phosphorylation-dependent regulation of smooth muscle myosin. *Biochemistry*, **37**, 13285–13290.
11. Trybus, K. M., Huiatt, T. W. & Lowey, S. (1982). A bent monomeric conformation of myosin from smooth muscle. *Proc. Natl Acad. Sci. USA*, **79**, 6151–6155.
12. Liu, J., Wendt, T., Taylor, D. & Taylor, K. (2003). Refined model of the 10 S conformation of smooth muscle myosin by cryo-electron microscopy 3D image reconstruction. *J. Mol. Biol.* **329**, 963–972.
13. Craig, R., Smith, R. & Kendrick-Jones, J. (1983). Light-chain phosphorylation controls the conformation of vertebrate non-muscle and smooth muscle myosin molecules. *Nature*, **302**, 436–439.
14. Wendt, T., Taylor, D., Messier, T., Trybus, K. M. & Taylor, K. A. (1999). Visualization of head–head interactions in the inhibited state of smooth muscle myosin. *J. Cell Biol.* **147**, 1385–1390.
15. Trybus, K. M. (1991). Assembly of cytoplasmic and smooth muscle myosin. *Curr. Opin. Cell Biol.* **3**, 105–111.
16. Szent-Gyorgyi, A. G., Kalabokis, V. N. & Perreault-Micale, C. L. (1999). Regulation by molluscan myosins. *Mol. Cell. Biochem.* **190**, 55–62.
17. Ankrett, R. J., Rowe, A. J., Cross, R. A., Kendrick-Jones, J. & Bagshaw, C. R. (1991). A folded (10 S) conformer of myosin from a striated muscle and its implications for regulation of ATPase activity. *J. Mol. Biol.* **217**, 323–335.
18. Jung, H. S., Burgess, S. A., Colegrave, M., Patel, H., Chantler, P. D., Chalovich, J. M. *et al.* (2004). Comparative studies of the folded structures of scallop striated and vertebrate smooth muscle myosins. *Biophys. J.* **86**, 403a.
19. Go, N., Noguti, T. & Nishikawa, T. (1983). Dynamics of a small globular protein in terms of low-frequency vibrational modes. *Proc. Natl Acad. Sci. USA*, **80**, 3696–3700.
20. Tama, F. & Sanejouand, Y. H. (2001). Conformational change of proteins arising from normal mode calculations. *Protein Eng.* **14**, 1–6.
21. Tama, F. (2003). Normal mode analysis with simplified models to investigate the global dynamics of biological systems. *Protein Pept. Letters*, **10**, 119–132.
22. Li, Y., Brown, J. H., Reshetnikova, L., Blazsek, A., Farkas, L., Nyitray, L. & Cohen, C. (2003). Visualization of an unstable coiled coil from the scallop myosin rod. *Nature*, **424**, 341–345.
23. Baker, T. S. & Johnson, J. E. (1996). Low resolution meets high: towards a resolution continuum from cells to atoms. *Curr. Opin. Struct. Biol.* **6**, 585–594.
24. Burgess, S., Yu, R., Walker, M. L., Trinick, J., Chalovich, J. M. & Knight, P. J. (2002). Structure of smooth muscle myosin in the switched-off state. *Biophys. J.* **82**, 356a.
25. Ikebe, M., Ikebe, R., Kamisoyama, H., Reardon, S., Schwonek, J. P., Sanders, C. R., II & Matsuura, M. (1994). Function of the NH2-terminal domain of the regulatory light chain on the regulation of smooth muscle myosin. *J. Biol. Chem.* **269**, 28173–28180.
26. McLachlan, A. D. & Karn, J. (1982). Periodic charge distributions in the myosin rod amino acid sequence match cross-bridge spacings in muscle. *Nature*, **299**, 226–231.
27. Miyashita, O., Onuchic, J. N. & Wolynes, P. G. (2003). Nonlinear elasticity, proteinquakes, and the energy landscapes of functional transitions in proteins. *Proc. Natl Acad. Sci. USA*, **100**, 12570–12575.
28. Asbury, C. L., Fehr, A. N. & Block, S. M. (2003). Kinesin moves by an asymmetric hand-over-hand mechanism. *Science*, **302**, 2130–2134.
29. Houdusse, A. & Cohen, C. (1996). Structure of the regulatory domain of scallop myosin at 2 Å resolution: implications for regulation. *Structure*, **4**, 21–32.
30. Rayment, I., Rypniewsky, W. R., Schmidt-Bäse, K., Smith, R., Tomchick, D. R., Benning, M. M. *et al.* (1993). Three-dimensional structure of myosin subfragment-1: a molecular motor. *Science*, **261**, 50–58.
31. Kammerer, R. A., Schulthess, T., Landwehr, R., Lustig, A., Engel, J., Aebi, U. & Steinmetz, M. O. (1998). An autonomous folding unit mediates the assembly of two-stranded coiled coils. *Proc. Natl Acad. Sci. USA*, **95**, 13419–13424.
32. Trybus, K. M. (1994). Regulation of expressed truncated smooth muscle myosins. Role of the essential light chain and tail length. *J. Biol. Chem.* **269**, 20819–20822.
33. Cohen, C. & Parry, D. A. (1990). Alpha-helical coiled coils and bundles: how to design an alpha-helical protein. *Proteins: Struct. Funct. Genet.* **7**, 1–15.
34. Zhang, Y., Shao, Z., Somlyo, A. P. & Somlyo, A. V. (1997). Cryo-atomic force microscopy of smooth muscle myosin. *Biophys. J.* **72**, 1308–1318.
35. Levine, B. A., Griffiths, H. S., Patchell, V. B. & Perry,

S. V. (1988). Study of the phosphorylatable light chains of skeletal and gizzard myosins by nuclear magnetic resonance spectroscopy. *Biochem. J.* **254**, 277–286.
36. Cross, R. A., Jackson, A. P., Citi, S., Kendrick-Jones, J. & Bagshaw, C. R. (1988). Active site trapping of nucleotide by smooth and non-muscle myosins. *J. Mol. Biol.* **203**, 173–181.
37. Cross, R. A., Cross, K. E. & Sobieszek, A. (1986). ATP-linked monomer–polymer equilibrium of smooth muscle myosin: the free folded monomer traps ADP.Pi. *EMBO J.* **5**, 2637–2641.
38. Kendrick-Jones, J., Smith, R. C., Craig, R. & Citi, S. (1987). Polymerization of vertebrate non-muscle and smooth muscle myosins. *J. Mol. Biol.* **198**, 241–252.
39. Ikebe, M., Yamada, M., Mabuchi, K., Kambara, T. & Ikebe, R. (1999). Registration of the rod is not critical for the phosphorylation-dependent regulation of smooth muscle myosin. *Biochemistry*, **38**, 10768–10774.
40. Feynman, R. P., Leighton, R. B. & Sands, M. (1964). *The Feynman Lectures on Physics*, Addison-Wesley Publishing Company, Inc, Reading, MA.
41. Cross, R. A. (1984). Bending of smooth muscle myosin rod. *FEBS Letters*, **176**, 197–201.
42. Trybus, K. M. (1989). Filamentous smooth muscle myosin is regulated by phosphorylation. *J. Cell Biol.* **109**, 2887–2894.
43. Wagner, P. D. & Vu, N. D. (1988). Filament assembly and regulation of the actin-activated ATPase activity of thymus myosin. *Biochemistry*, **27**, 6236–6242.
44. Wagner, P. D. & Vu, N. D. (1987). Actin-activation of unphosphorylated gizzard myosin. *J. Biol. Chem.* **262**, 15556–15562.
45. Wagner, P. D. & Vu, N. D. (1986). Regulation of the actin-activated ATPase of aorta smooth muscle myosin. *J. Biol. Chem.* **261**, 7778–7783.
46. Wagner, P. D. & George, J. N. (1986). Phosphorylation of thymus myosin increases its apparent affinity for actin but not its maximum adenosinetriphosphatase rate. *Biochemistry*, **25**, 913–918.
47. McLachlan, A. D. & Karn, J. (1983). Periodic features in the amino acid sequence of nematode myosin rod. *J. Mol. Biol.* **164**, 605–626.
48. Ikebe, M., Hinkins, S. & Hartshorne, D. J. (1983). Correlation of enzymatic properties and conformation of smooth muscle myosin. *Biochemistry*, **22**, 4580–4587.
49. Frado, L.-L.Y. & Craig, R. (1992). Structural changes induced in scallop heavy meromyosin molecules by Ca^{2+} and ATP. *J. Muscle Res. Cell Motil.* **13**, 436–446.
50. Takahashi, T., Fukukawa, C., Naraoka, C., Katoh, T. & Yazawa, M. (1999). Conformations of vertebrate striated muscle myosin monomers in equilibrium with filaments. *J. Biochem. (Tokyo)*, **126**, 34–40.
51. AL-Khayat, H. A., Hudson, L., Reedy, M. K., Irving, T. C. & Squire, J. M. (2003). Myosin head configuration in relaxed insect flight muscle: X-ray modelled resting crossbridges in a pre-powerstroke state are poised for actin binding. *Biophys. J.* **85**, 1063–1079.
52. Padron, R., Alamo, L., Murgich, J. & Craig, R. (1998). Towards an atomic model of the thick filaments of muscle. *J. Mol. Biol.* **275**, 35–41.
53. Crowther, R. A., Padron, R. & Craig, R. (1985). Arrangement of the heads of myosin in relaxed thick filaments from tarantula muscle. *J. Mol. Biol.* **184**, 429–439.
54. Stewart, M., Kensler, R. W. & Levine, R. J. (1985). Three-dimensional reconstruction of thick filaments from Limulus and scorpion muscle. *J. Cell Biol.* **101**, 402–411.
55. Stewart, M. & Kensler, R. W. (1986). Arrangement of myosin heads in relaxed thick filaments from frog skeletal muscle. *J. Mol. Biol.* **192**, 831–851.
56. Vibert, P. (1992). Helical reconstruction of frozen-hydrated scallop myosin filaments. *J. Mol. Biol.* **223**, 661–671.
57. Craig, R. & Megerman, J. (1977). Assembly of smooth muscle myosin into side-polar filaments. *J. Cell Biol.* **75**, 990–996.
58. Cooke, P. H., Fay, F. S. & Craig, R. (1989). Myosin filaments isolated from skinned amphibian smooth muscle cells are side-polar. *J. Muscle Res. Cell Motil.* **10**, 206–220.
59. Xu, J. Q., Harder, B. A., Uman, P. & Craig, R. (1996). Myosin filament structure in vertebrate smooth muscle. *J. Cell Biol.* **134**, 53–66.
60. Liu, J., Reedy, M. C., Goldman, Y. E., Franzini-Armstrong, C., Sasaki, H., Tregear, R. T. *et al*. (2004). Electron tomography of fast frozen, stretched rigor fibers reveals elastic distortions in the myosin cross-bridges. *J. Struct. Biol.* **147**, 268–282.
61. Cross, R. A., Geeves, M. A. & Kendrick-Jones, J. (1991). A nucleation–elongation mechanism for the self-assembly of side polar sheets of smooth muscle myosin. *EMBO J.* **10**, 747–756.
62. Somlyo, A. P., Somlyo, A. V., Kitazawa, T., Bond, M., Shuman, H. & Kowarski, D. (1983). Ultrastructure, function and composition of smooth muscle. *Ann. Biomed. Eng.* **11**, 579–588.
63. Katayama, E., Scott-Woo, G. & Ikebe, M. (1995). Effect of caldesmon on the assembly of smooth muscle myosin. *J. Biol. Chem.* **270**, 3919–3925.
64. Shirinsky, V. P., Vorotnikov, A. V., Birukov, K. G., Nanaev, A. K., Collinge, M., Lukas, T. J. *et al*. (1993). A kinase-related protein stabilizes unphosphorylated smooth muscle myosin minifilaments in the presence of ATP. *J. Biol. Chem.* **268**, 16578–16583.
65. Chakrabarty, T., Yengo, C., Baldacchino, C., Chen, L. Q., Sweeney, H. L. & Selvin, P. R. (2003). Does the S2 rod of myosin II uncoil upon two-headed binding to actin? A leucine-zippered HMM study. *Biochemistry*, **42**, 12886–12892.
66. Taylor, K. A., Schmitz, H., Reedy, M. C., Goldman, Y. E., Franzini-Armstrong, C., Sasaki, H. *et al*. (1999). Tomographic 3-D reconstruction of quick frozen, Ca^{2+}-activated contracting insect flight muscle. *Cell*, **99**, 421–431.
67. Tregear, R. T., Reedy, M. C., Goldman, Y. E., Taylor, K. A., Winkler, H., Franzini-Armstrong, C. *et al*. (2004). Cross-bridge number, position, and angle in target zones of cryofixed isometrically active insect flight muscle. *Biophys. J.* **86**, 3009–3019.
68. Cooke, R. & Franks, K. E. (1978). Generation of force by single-headed myosin. *J. Mol. Biol.* **120**, 361–373.
69. Harada, Y., Noguchi, A., Kishino, A. & Yanagida, T. (1987). Sliding movement of single actin filaments on one-headed myosin filaments. *Nature*, **326**, 805–808.
70. Tyska, M. J., Dupuis, D. E., Guilford, W. H., Patlak, J. B., Waller, G. S., Trybus, K. M. *et al*. (1999). Two heads of myosin are better than one for generating force and motion. *Proc. Natl Acad. Sci. USA*, **96**, 4402–4407.
71. Kad, N. M., Rovner, A. S., Fagnant, P. M., Joel, P. B., Kennedy, G. G., Patlak, J. B. *et al*. (2003). A mutant heterodimeric myosin with one inactive head generates maximal displacement. *J. Cell Biol.* **162**, 481–488.

72. Conibear, P. B. & Geeves, M. A. (1998). Cooperativity between the two heads of rabbit skeletal muscle heavy meromyosin in binding to actin. *Biophys. J.* **75**, 926–937.
73. Woehlke, G. & Schliwa, M. (2000). Walking on two heads: the many talents of kinesin. *Nature Rev. Mol. Cell Biol.* **1**, 50–58.
74. Hua, W., Chung, J. & Gelles, J. (2002). Distinguishing inchworm and hand-over-hand processive kinesin movement by neck rotation measurements. *Science*, **295**, 844–848.
75. Reck-Peterson, S. L., Tyska, M. J., Novick, P. J. & Mooseker, M. S. (2001). The yeast class V myosins, Myo2p and Myo4p, are nonprocessive actin-based motors. *J. Cell Biol.* **153**, 1121–1126.
76. Wang, F., Chen, L., Arcucci, O., Harvey, E. V., Bowers, B., Xu, Y. *et al*. (2000). Effect of ADP and ionic strength on the kinetic and motile properties of recombinant mouse myosin V. *J. Biol. Chem.* **275**, 4329–4335.
77. Dominguez, R., Freyzon, Y., Trybus, K. M. & Cohen, C. (1998). Crystal structure of a vertebrate smooth muscle myosin motor domain and its complex with the essential light chain: visualization of the pre-power stroke state. *Cell*, **94**, 559–571.
78. Butler, B. A. (1998). Sequence analysis using GCG. *Methods Biochem. Anal.* **39**, 74–97.
79. Kolinski, A., Jaroszewski, L., Rotkiewicz, P. & Skolnick, J. (1998). An efficient monte carlo model of protein chains. Modelling the short-range correlations between side group centers of mass. *J. Phys. Chem. B*, **102**, 4628–4637.
80. Feig, M., Karanicolas, J. & Brooks, C. L., III (2004). MMTSB Tool Set: enhanced sampling and multiscale modelling methods for applications in structural biology. *J. Mol. Graph. Model.* **22**, 377–395.
81. Lee, M. S., Feig, M., Salsbury, F. R., Jr & Brooks, C. L., III (2003). A new analytical approximation to the standard molecular volume definition and its application to generalized Born calculations. *J. Comput. Chem.* **24**, 1348–1356.
82. Offer, G. & Sessions, R. (1995). Computer modelling of the α-helical coiled coil: packing of side-chains in the inner core. *J. Mol. Biol.* **249**, 967–987.
83. Berger, B., Wilson, D. B., Wolf, E., Tonchev, T., Milla, M. & Kim, P. S. (1995). Predicting coiled coils by use of pairwise residue correlations. *Proc. Natl Acad. Sci. USA*, **92**, 8259–8263.
84. Lupas, A., Van Dyke, M. & Stock, J. (1991). Predicting coiled coils from protein sequences. *Science*, **252**, 1162–1164.
85. Brooks, B. R., Bruccoleri, R. E., Olafson, B. D., States, D. J., Swaminathan, S. & Karplus, M. (1983). CHARMM: a program for macromolecular energy, minimization, and dynamics calculations. *J. Comput. Chem.* **4**, 187–217.
86. Rost, B. & Liu, J. (2003). The predict protein server. *Nucl. Acids Res.* **31**, 3300–3304.
87. Kneller, D. G., Cohen, F. E. & Langridge, R. (1990). Improvements in protein secondary structure prediction by an enhanced neural network. *J. Mol. Biol.* **214**, 171–182.
88. Tama, F., Valle, M., Frank, J. & Brooks, C. L., III (2003). Dynamic reorganization of the functionally active ribosome explored by normal mode analysis and cryo-electron microscopy. *Proc. Natl Acad. Sci. USA*, **100**, 9319–9323.
89. Tirion, M. M. (1996). Large amplitude elastic motions in proteins from a single-parameter, atomic analysis. *Phys. Rev. Letters*, **77**, 1905–1908.
90. Atilgan, A. R., Durell, S. R., Jernigan, R. L., Demirel, M. C., Keskin, O. & Bahar, I. (2001). Anisotropy of fluctuation dynamics of proteins with an elastic network model. *Biophys. J.* **80**, 505–515.
91. Tama, F., Miyashita, O. & Brooks, C. L., III (2004). Flexible multi-scale fitting of atomic structures into low-resolution electron density maps with elastic network normal mode analysis. *J. Mol. Biol.* **337**, 985–999.
92. Kraulis, P. J. (1991). MolScript: a program to produce both detailed and schematic plots of protein structures. *J. Appl. Crystallog.* **24**, 946–950.
93. Humphrey, W., Dalke, A. & Schulten, K. (1996). VMD: visual molecular dynamics. *J. Mol. Graph. Model.* **33–38**, 27–28.
94. Esnouf, R. M. (1997). An extensively modified version of MolScript that includes greatly enhanced coloring capabilities. *J. Mol. Graph. Model.* **15**, 132–134.

Edited by M. Moody

(Received 30 July 2004; received in revised form 28 October 2004; accepted 28 October 2004)